REPORT 1086

ANALYSIS OF THE EFFECTS OF WING INTERFERENCE ON THE TAIL CONTRIBUTIONS TO THE ROLLING DERIVATIVES[1]

By William H. Michael, Jr.

SUMMARY

An analysis of the effects of wing interference on the tail contributions to the rolling stability derivatives of complete airplane configurations is made by calculating the angularity of the air stream at the vertical tail due to rolling and determining the resulting forces and moments. Some of the important factors which affect the resultant angularity on the vertical tail are wing aspect ratio and sweepback, vertical-tail span, and considerations associated with angle of attack and airplane geometry.

Some calculated sidewash results for a limited range of wing plan forms and vertical-tail sizes are presented. Equations taking into account the sidewash results are given for determining the tail contributions to the rolling derivatives.

Comparisons of estimated and experimental results indicate that a consideration of wing interference effects improves the estimated values of the tail contributions to the rolling derivatives and that fair agreement with available experimental data is obtained.

INTRODUCTION

Dynamic-stability calculations have shown that, under certain conditions, important changes in the characteristics of the lateral oscillation might result from small changes in the rotary stability derivatives. This effect has been noted especially in the changes in damping of the lateral oscillation due to changes in the yawing-moment-due-to-roll parameter C_{n_p}. In view of these variations in calculated results, the estimations of the rotary derivatives should be as accurate as possible. This report presents a correction to the present methods of estimating the tail contributions to the rolling derivatives.

The generally accepted methods for estimating tail contributions to the rolling derivatives, as presented in reference 1, make use of the assumption that interference effects of component parts of the airplane can be neglected. Calculations using the methods of reference 1 have been found to agree well with experimental data for wing-off configurations, but some data (see reference 2) indicate that the calculations differ considerably from the measured values for the wing-on configurations. The data indicate that the interference effects of the wing on the tail surfaces account for a large part of the discrepancy between the measured and estimated parameters.

This report presents calculations of the angularity of the air stream with respect to the vertical tail for a rolling airplane, the interference effects of the wing being taken into account. A discussion of the factors which enter into the calculations is given and equations for applying the sidewash results to the determination of the tail contributions to the rolling-stability derivatives are included. The results are compared with some available experimental data.

SYMBOLS AND COEFFICIENTS

The positive directions of forces, angles, and moments are shown in figure 1 (a). The symbols used herein are defined as follows:

A	aspect ratio (b^2/S)
α	airplane angle of attack, degrees
α_{V_p}	angularity of air stream at vertical tail, positive in such direction as to give positive side force, radians
b	wing span, feet
b_V	vertical-tail span, feet
c	local wing chord, feet
$\bar{c}$	wing mean geometric chord, feet
c_V	local vertical-tail chord, feet
Γ	wing circulation, square feet per second
ϵ	angle of downwash, angle measured in xz-plane between trailing vortex sheet and longitudinal stability axis, radians
h	distance, measured in xz-plane, perpendicular to longitudinal stability axis (axis of rotation), positive above longitudinal axis, feet (fig. 1 (b))
$\bar{h}$	perpendicular distance, measured in xz-plane, from airplane reference axis to center of pressure of vertical tail, positive above reference axis, feet
h_t	distance, measured in xz-plane, perpendicular to trailing vortex sheet at tail, positive above vortex sheet, feet
h_r	distance, measured in xz-plane, perpendicular to vertical-tail root, positive above root, feet
h_1	perpendicular displacement of vortex sheet at tail with angle of attack, measured in xz-plane, positive above longitudinal axis, feet

[1] Supersedes NACA TN 2332, "Analysis of the Effects of Wing Interference on the Tail Contributions to the Rolling Derivatives" by William H. Michael, Jr., 1951.

272483—54——37

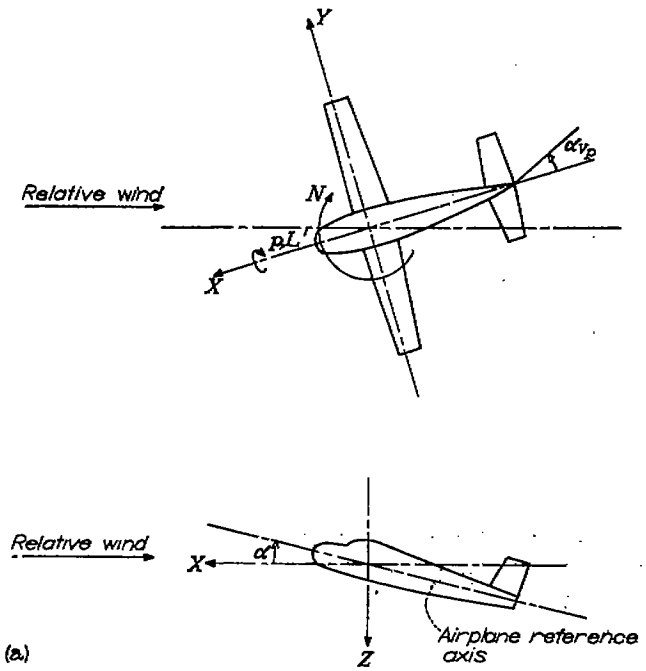

(a) Notations for the stability system of axes.

FIGURE 1.—Notations for the axis system and illustration of some important symbols.

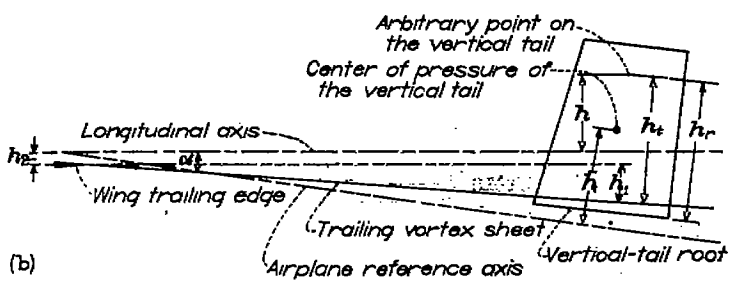

(b) Illustration of symbols used in referring to the trailing vortex sheet and the vertical tail.

FIGURE 1.—Concluded.

h_2 perpendicular displacement of vortex sheet at tail (that is, wing trailing edge) with respect to longitudinal axis at $\alpha=0°$, positive above longitudinal axis, feet

η component of angularity of flow at vertical tail resulting from rolling motion of tail, positive in such direction as to give positive side force, radians

l_n longitudinal distance, measured parallel to airplane reference axis, from assumed lifting line at any spanwise station to center of pressure of vertical tail (assumed equal to l_t for unswept wings), feet

l_t tail length, longitudinal distance, measured parallel to airplane reference axis, from airplane center of gravity to center of pressure of vertical tail, feet

L' rolling moment

Λ angle of sweepback of lifting line, degrees

λ taper ratio

N yawing moment

p rolling angular velocity, radians per second

$\frac{pb}{2V}$ rolling-velocity parameter

q induced velocity, feet per second

r perpendicular distance from a line vortex to point at which induced velocity is to be found, feet

ρ mass density of air, slugs per cubic foot

S_V vertical-tail area, square feet

S_W wing area, square feet

σ sidewash angle, component of angularity of flow at vertical tail resulting from interference effect of wing, positive for positive side force, radians

$\left(\frac{\partial\sigma}{\partial\frac{pb}{2V}}\right)_{av}$ average value of $\frac{\partial\sigma}{\partial\frac{pb}{2V}}$ on the vertical tail

v lateral velocity, feet per second

V free-stream velocity, feet per second

x distance along longitudinal axis, feet

y distance from plane of symmetry to spanwise location of trailing vortices, feet

X longitudinal force

Y lateral force

Z normal force

θ, θ_1, ψ variables used in development (fig. 3 (a))

c_l section lift coefficient $\left(\frac{\text{Section lift}}{\frac{1}{2}\rho V^2 c}\right)$

$(c_{l_\alpha})_V$ section lift-curve slope of vertical tail

$\frac{cc_l}{\bar{c}\frac{pb}{2V}}$ spanwise loading coefficient for unit $\frac{pb}{2V}$

$(C_{L_\alpha})_V$ lift-curve slope of vertical tail, per radian

C_l rolling-moment coefficient $\left(\frac{L'}{\frac{1}{2}\rho V^2 S b}\right)$

C_n yawing-moment coefficient $\left(\frac{N}{\frac{1}{2}\rho V^2 S b}\right)$

C_Y lateral-force coefficient $\left(\frac{Y}{\frac{1}{2}\rho V^2 S}\right)$

$C_{l_p}=\frac{\partial C_l}{\partial\frac{pb}{2V}}$

$C_{n_p}=\frac{\partial C_n}{\partial\frac{pb}{2V}}$

$C_{Y_p}=\frac{\partial C_Y}{\partial\frac{pb}{2V}}$

$(C_{l_p})_t$ vertical-tail contribution to C_{l_p}

$(C_{n_p})_t$ vertical-tail contribution to C_{n_p}

$(C_{Y_p})_t$ vertical-tail contribution to C_{Y_p}

Subscript:

n denotes a particular line vortex

ANALYSIS

GENERAL REMARKS

The first objective is to find the angularity of the air stream of a rolling airplane with respect to the vertical tail, without accounting for the effects of the fuselage and the horizontal tail. The angularity is considered herein to be composed of two parts—the sidewash angle induced by the antisymmetrical load distribution on the rolling wing and the geometric angle caused by the rolling motion of the isolated vertical tail. Expressions for these two components of the angularity are given in this section. The sidewash-angle calculations are given for straight wings and a discussion is given subsequently concerning additional considerations for swept wings. Simplified methods are used in the derivations and calculations when little loss in accuracy is incurred.

In the calculations for the sidewash induced by the rolling wing and in the application of the calculations, several assumptions are made concerning the trailing vortex sheet. These assumptions pertain to the rolling-up, vertical displacement, and twisting, or rotation, of the trailing vortex sheet.

In downwash calculations for lifting wings of high aspect ratio, the assumption has generally been accepted that the distortion of the trailing vortex sheet in the vicinity of the tail may be accounted for by considering a flat vortex sheet displaced vertically by an amount equal to the displacement of the center of the actual vortex sheet at the plane of symmetry and neglecting the rolling-up of the sheet (reference 3). The hypothesis that the trailing vortex sheet remains flat will be assumed to apply equally well to the calculation of the sidewash for a rolling wing. There might be some doubt as to the validity of the assumption at low aspect ratios, since the distance behind the wing for complete rolling-up is proportional to the aspect ratio (reference 4) and is also inversely proportional to the lift coefficient. Experimental data in reference 3 indicate that, for a value of less than 45 percent for the ratio of distance of the tail behind the wing to the distance behind the wing for complete rolling-up of the vortices, the assumption for the displaced vortex sheet holds very well for the downwash calculations. For the fairly extreme case of an aspect-ratio-3 wing at a lift coefficient of 0.4, complete rolling-up would occur at about 4.2 semispans and thus the ratio (0.45) would be obtained for a tail length of about 1.9 semispans. In general, the majority of the cases considered can be expected to fall within the 45-percent limit and the assumption of the flat trailing vortex sheet can be justified.

The displacement of the assumed flat vortex sheet from the wing trailing edge, at a distance x behind the wing trailing edge, which is the displacement of the actual vortex sheet at the plane of symmetry, is found from reference 3 to be

$$h_1=\int_{T.E.}^{x} \tan \epsilon \, dx \tag{1}$$

As an approximation, ϵ is considered constant and the displacement of the vortex sheet at the tail may be expressed in semispans as

$$\frac{h_1}{b/2}=-\frac{l_t}{b/2}\tan \epsilon \tag{2}$$

The rotation of the trailing vortex sheet at the tail location is a function of the tail length, airplane velocity, and the rolling angular velocity; that is, the rotation is approximately equal to $\frac{pb}{2V}\frac{l_t}{b/2}$. For a tail length of the order of the wing semispan and for the usual values of $pb/2V$ encountered, the rotation of the vortex sheet at the tail location would be less than 0.1 radian. The change in sidewash induced at the vertical tail by this amount of rotation would be negligible.

CALCULATION OF THE ANGULARITY OF FLOW AT THE VERTICAL TAIL

Sidewash angle induced by the rolling wing.—The sidewash, induced by the antisymmetrical load distribution of a rolling wing, is calculated by using the concept of a lifting line with trailing vortices extending downstream to infinity. The load distribution on the semispan is represented by a number of horseshoe vortices with the bound vortices concentrated at the wing quarter-chord line, as shown for a straight wing in figure 2. The bound vortices for the straight wing produce no component of sidewash; so the trailing vortices are the only ones to be considered. The derivation for the sidewash is made for points in the plane of symmetry at perpendicular distances with respect to the vortex sheet and considerations associated with vortex-sheet displacement are discussed subsequently.

The velocity induced at a point P by a straight-line vortex filament, as given by the Biot-Savart equation, is

$$q=\frac{\Gamma_n}{4\pi r_n}\int_{\theta_n}^{\pi-\theta_{1_n}} \sin \theta \, d\theta=\frac{\Gamma_n}{4\pi r_n}(\cos \theta_{1_n}+\cos \theta_n) \tag{3}$$

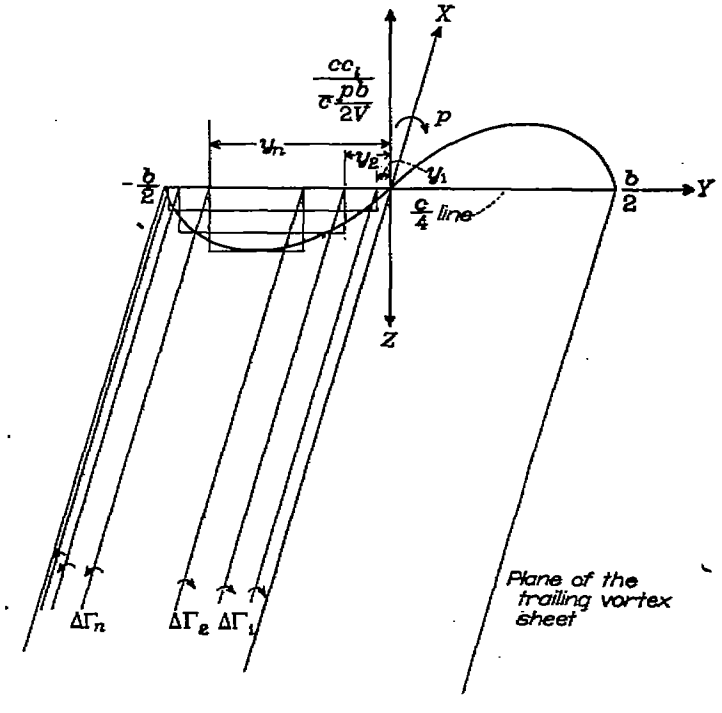

FIGURE 2.—The load distribution on a rolling wing and the method of approximating the loading with a finite number of vortices.

(See fig. 3 (a) for definitions and notation.) If semi-infinite vortex filaments are considered, then $\theta_1 \approx 0$ and

$$q=\frac{\Gamma_n}{4\pi r_n}(1+\cos\theta_n) \tag{4}$$

From a consideration of the Kutta-Joukowski law and Helmholtz's vortex theorems, the strength of the trailing vortices can be shown to be related to the change in section lift along the span by the equation

$$\Delta\Gamma=\Delta\left(\frac{cc_l}{2}\right)V \tag{5}$$

In reference 5, the lift distributions due to roll for a series of wings are given in terms of the spanwise loading coefficient for unit wing-tip helix angle and are expressed as $\frac{cc_l}{\bar{c}\frac{pb}{2V}}$. The strength of the trailing vortices for unit $\frac{pb}{2V}$, expressed in terms of this parameter, becomes

$$\frac{\Delta\Gamma}{\frac{pb}{2V}}=\Delta\left(\frac{cc_l}{\bar{c}\frac{pb}{2V}}\right)\frac{\bar{c}V}{2} \tag{6}$$

The induced velocity at the point P is the summation of the velocities induced by all the trailing vortices. The total induced velocity is

$$q=\sum_{n=1}^{2n}\frac{\Delta\left(\frac{cc_l}{\bar{c}\frac{pb}{2V}}\right)_n\frac{\bar{c}}{2}V}{4\pi r_n}(1+\cos\theta_n) \tag{7}$$

where n denotes the number and position of the trailing vortices over the semispan of the wing. Since the loading on a rolling wing is antisymmetrical, the induced sidewash velocities from both semispans are in the same direction and equal at the plane of symmetry; hence, only the loading for one semispan need be considered and the results doubled. The lateral component of the induced velocity in planes parallel to the trailing vortex sheet is

$$v=2q\sin\psi=2\sum_{1}^{n}\frac{\Delta\left(\frac{cc_l}{\bar{c}\frac{pb}{2V}}\right)_n\frac{\bar{c}}{2}V}{4\pi r_n}\sin\psi_n(1+\cos\theta_n) \tag{8}$$

where $\sin\psi_n=\frac{h_t}{\sqrt{h_t^2+y_n^2}}$, as shown in figure 3 (a). The sidewash angle at P, expressed in radians, is

$$\frac{v}{V}=2\sum_{n=1}^{n}\frac{\Delta\left(\frac{cc_l}{\bar{c}\frac{pb}{2V}}\right)_n\frac{\bar{c}}{2}}{4\pi r_n}\sin\psi_n(1+\cos\theta_n) \tag{9}$$

Upon substitution of the relations

$$r_n=\sqrt{h_t^2+y_n^2}$$

$$\sin\psi_n=\frac{h_t}{\sqrt{h_t^2+y_n^2}}$$

and

$$\cos\theta_n=\frac{l_t}{\sqrt{l_t^2+y_n^2+h_t^2}}$$

into equation (9), the expression for the sidewash angle at any point in the plane of symmetry is found to be

$$\frac{v}{V}=2\sum_{n=1}^{n}\frac{\Delta\left(\frac{cc_l}{\bar{c}\frac{pb}{2V}}\right)_n\frac{\bar{c}}{2}h_t}{4\pi(h_t^2+y_n^2)}\left(1+\frac{l_t}{\sqrt{l_t^2+y_n^2+h_t^2}}\right) \tag{10}$$

The equation can be made nondimensional and, when the definition $A=\frac{b}{\bar{c}}$ is used, the final equation for the sidewash induced at the tail by the rolling wing for unit $\frac{pb}{2V}$ is

$$\frac{\partial\sigma}{\partial\frac{pb}{2V}}=\frac{1}{2\pi A}\sum_{n=1}^{n}\frac{\Delta\left(\frac{cc_l}{\bar{c}\frac{pb}{2V}}\right)_n\frac{h_t}{b/2}}{\left(\frac{y_n}{b/2}\right)^2+\left(\frac{h_t}{b/2}\right)^2}\left[1+\frac{\frac{l_t}{b/2}}{\sqrt{\left(\frac{l_t}{b/2}\right)^2+\left(\frac{y_n}{b/2}\right)^2+\left(\frac{h_t}{b/2}\right)^2}}\right] \tag{11}$$

Since the axis of rotation is the longitudinal axis, the sidewash at any distance $\frac{h}{b/2}$ with respect to the longitudinal axis is that calculated at the position $h_t=(h-h_1-h_2)$, where h_1 is the displacement of the vortex sheet with angle of attack and h_2 is the displacement of the vortex sheet with respect to the longitudinal axis for $\alpha=0°$. (See fig. 1 (b).)

Geometric angle caused by rolling motion of isolated vertical tail.—The angle induced at the vertical tail due to the rolling motion of the isolated vertical tail is proportional to the rolling velocity and the height above the axis of roll, as shown in figure 3 (b). The lateral velocity is

$$v=-ph=-\frac{pb}{2V}\frac{2V}{b}h \tag{12}$$

The angle induced by the rolling tail for unit $\frac{pb}{2V}$ is

$$\frac{\partial\eta}{\partial\frac{pb}{2V}}=\frac{v}{V}=-\frac{h}{b/2} \tag{13}$$

CONSIDERATIONS FOR NUMERICAL CALCULATIONS

The resultant local angularity along the span of the vertical tail is given by the sum of expressions (11) and (13). The

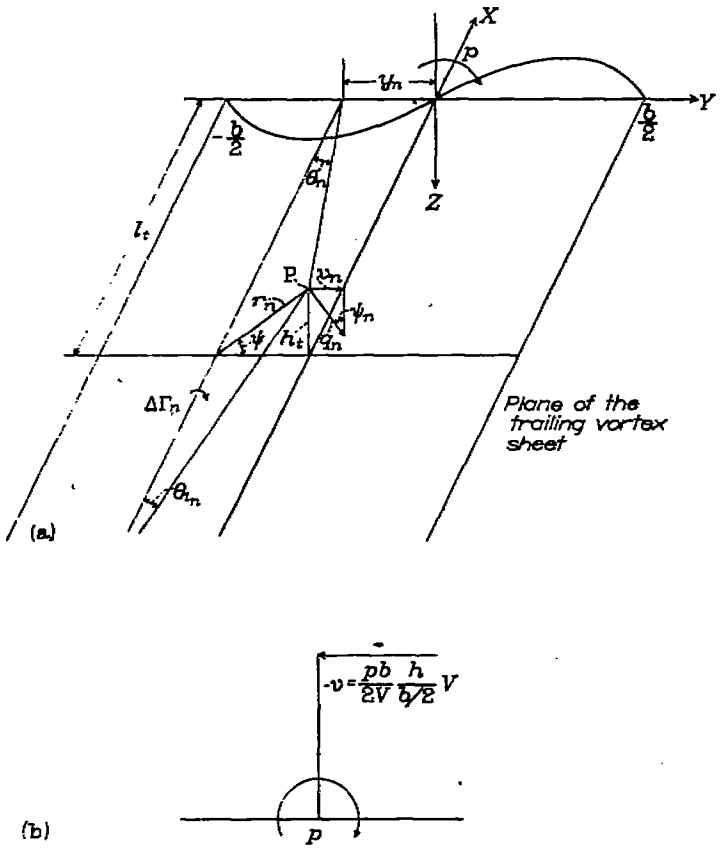

(a) Wing contribution.
(b) Tail contribution.

FIGURE 3.—Symbols and notation used in the calculation of the angularity at the vertical tail.

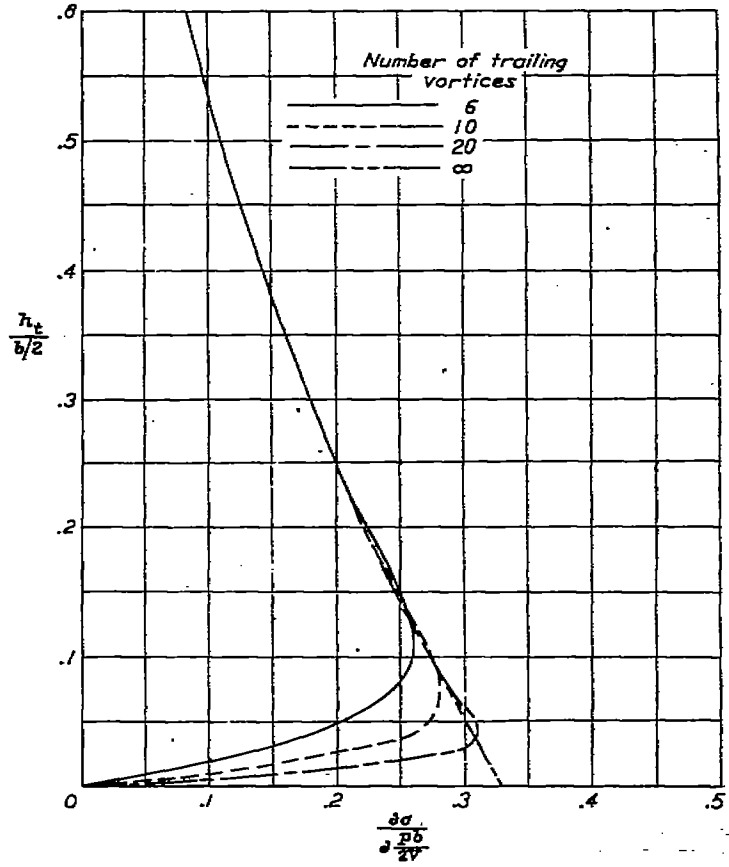

FIGURE 4.—Sidewash results using different numbers of trailing vortices.
$A=6.0$; $\lambda=1.0$; $\Lambda=0°$; $\frac{l_t}{b/2}=1.0$; $\alpha=0°$.

calculation of the sidewash velocity induced by the rolling wing (equation (11)) necessitates a knowledge of the spanwise loading distribution for the rolling wing. For the wings considered herein, the spanwise load distributions of reference 5 were approximated by a finite number of trailing vortices. The results of calculations using 6, 10, and 20 vortices per semispan and a continuous vortex distribution (loading represented by an analytical expression) are shown in figure 4 for a wing with $A=6.0$. The calculations using the finite numbers of vortices gave the same results as the continuous distribution except at small distances above the vortex sheet. Calculations for a lower aspect ratio ($A=3.0$) gave results similar to those for the $A=6.0$ wing in figure 4. The viscous properties of air are believed to be such as to prevent a sharp change in the sidewash at the vortex sheet such as that given by the calculations for the continuous distribution. Thus a rounding-off of the sidewash-angle curve near the vortex sheet appears to be a good approximation to the actual conditions. In the application of the sidewash results, the difference in using the curves for 6, 10, or 20 vortices would not be appreciable. From a consideration of the general appearance of the curve for 10 trailing vortices and the comparative time involved in the calculations, it was decided to use 10 vortices to approximate the loading.

Some measured values of the sidewash, from reference 2, are compared with the calculated values in figure 5. It should be pointed out that the sidewash measurements were made with the wing alone, so that there are no fuselage interference effects, although there might be some small support-strut interference. Fuselage interference effects are not accounted for in the calculations; so that comparison in figure 5 gives a good check on the method. A comparison of the resultant angularity and the rolling-tail induced-angle distributions shown in figure 5 gives an indication of the change in the appearance of the angularity distribution when the sidewash effect is included.

DISCUSSION

The variation of the resultant air-stream angularity along the vertical tail is determined from the general expressions for the angularity at any perpendicular distance with respect to the longitudinal axis (equations (11) and (13)) when the location of the vertical tail with respect to the longitudinal axis is known. This resultant angularity on the tail is dependent upon the magnitude of the sidewash and the locations of the sidewash and isolated rolling-tail geometric-angle distributions with respect to the vertical tail. Some factors which affect the magnitude of the sidewash and the locations of the sidewash and the rolling-tail geometric-angle distributions with respect to the vertical tail are discussed in this section.

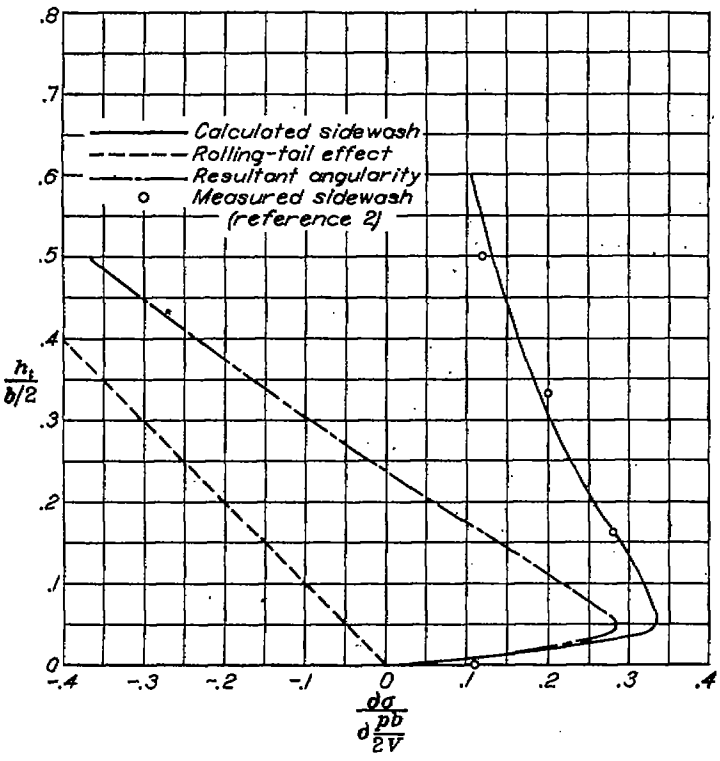

FIGURE 5.—Comparison of measured and calculated values of the sidewash-angle distribution, with rolling-tail angularity and resultant angularity distributions included. $A=4.0$; $\lambda=0.5$; $\Lambda=0°$; $\frac{l_t}{b/2}=0.85$; $\alpha=0°$.

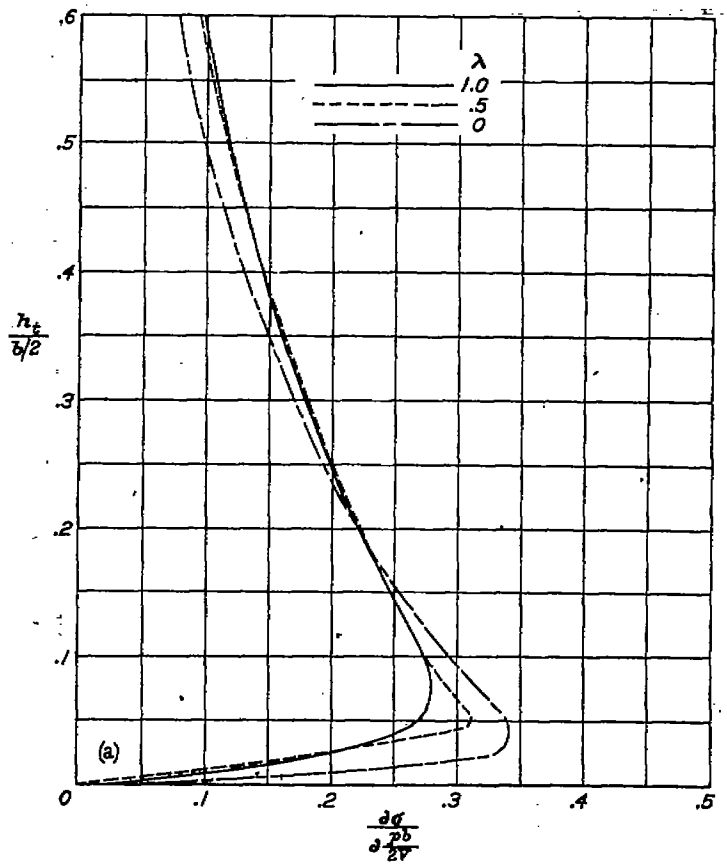

(a) $A=6.0$.

FIGURE 6.—Results of sidewash calculations for wings with various aspect ratios and taper ratios. $\Lambda=0°$; $\frac{l_t}{b/2}=1.0$; $\alpha=0°$.

FACTORS WHICH AFFECT THE MAGNITUDE OF THE SIDEWASH

Aspect ratio.—A consideration of equation (11) indicates that the aspect ratio enters into the sidewash calculations directly, as the reciprocal, and indirectly in the expression for the trailing vortex strength, which is a function of the loading on the rolling wing. For the high aspect ratios, the load distribution due to rolling is greater than for the low aspect ratios for unit $\frac{pb}{2V}$, but the reciprocal of the aspect ratio is the predominant factor and the sidewash increases by a considerable amount as the aspect ratio decreases. The results of calculations for several aspect ratios are shown in figure 6, in which the change in sidewash angle for unit $\frac{pb}{2V}$ is plotted against vertical displacement in semispans with respect to the vortex sheet. For very low aspect ratios (that is, 1.5 or 2.0) it is not known whether the assumptions pertaining to the rolling-up of the vortex sheet are valid, but nevertheless the sidewash calculations for $A=1.5$ are presented for completeness.

Taper ratio.—Taper ratio manifests itself in the distribution of the loading over the span of the wing and thus enters into equation (11) in the expression for the trailing vortex strength. The effect of changes in taper ratio is shown in figure 6 and is seen to be small. Decreasing the taper ratio usually results in a more positive sidewash-angle distribution at small distances above the trailing vortex sheet and in a less positive sidewash-angle distribution at larger distances above the vortex sheet.

Angle of sweep.—In considering the angle of sweep in the sidewash calculations, it is assumed that the loading of the wing may be considered to be concentrated on a swept lifting line. The bound vortices must be considered since they now produce a lateral component of induced velocity. The sidewash due to the trailing vortices is calculated in the same manner as for a straight wing, with due consideration given to the distances from the lifting line to the vertical-tail center of pressure at the spanwise location of the trailing vortices (that is, l_n instead of l_t in equation (11)). For wings with constant aspect ratio, the antisymmetrical loading decreases as the sweep angle is increased; hence, the strength of the trailing vortices decreases with increasing sweep angle.

The contribution of the bound vortices to the sidewash at the vertical tail is calculated in much the same manner as that due to the trailing vortices, the only difference being that consideration of the swept bound vortices modifies the geometrical factors in equation (3). The bound vortices become of increased importance for larger sweep angles, but for sweep angles as high as 60° and with normal tail lengths, the contribution of the bound vortices to the effective sidewash angle is found to be of the order of only about 10 percent.

In order to establish an approximate method for estimating the sidewash results for swept wings, calculations were made for swept wings of several aspect ratios and sweep angles. These calculations were compared with results for unswept

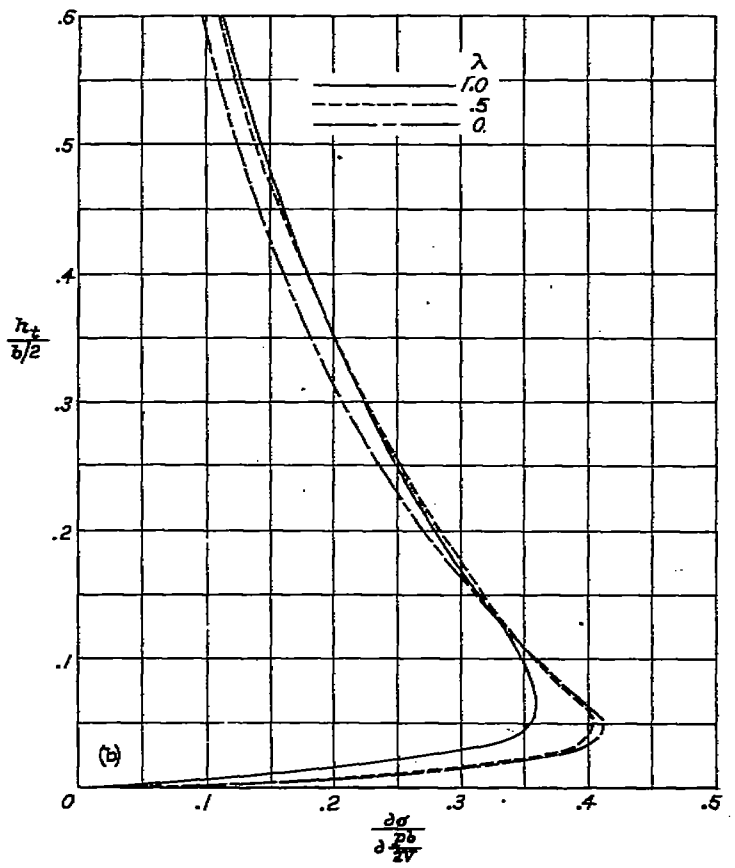

(b) $A=3.5$.

FIGURE 6.—Continued.

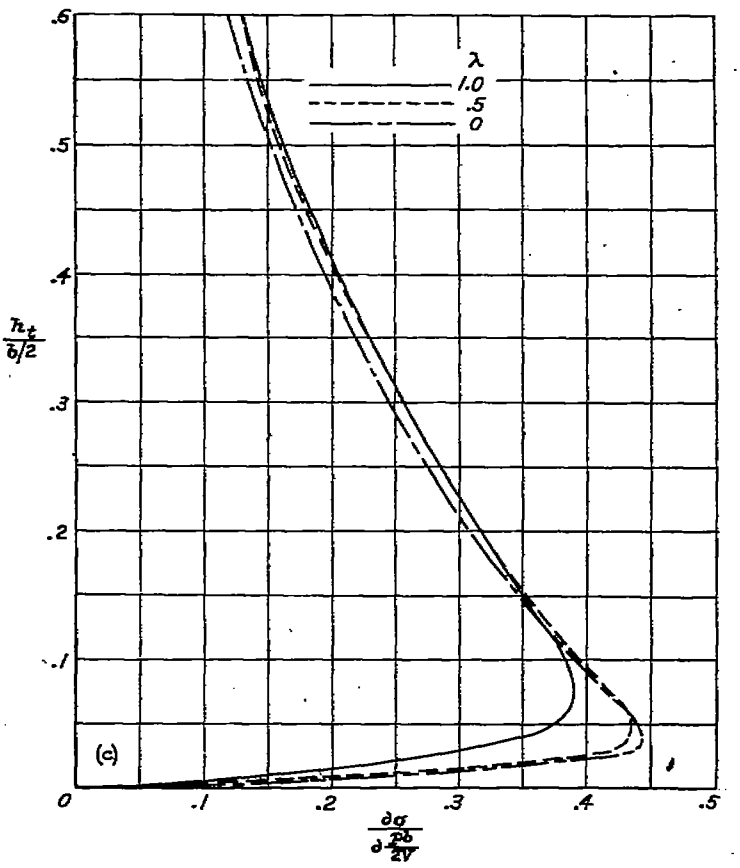

(c) $A=1.5$.

FIGURE 6.—Concluded.

wings of the same aspect ratio after the unswept-wing results had been reduced by the ratio of the damping-in-roll parameters for the swept and the unswept wings. Calculated results and approximated results for 60° sweptback wings with taper ratios of 0.5 are shown in figure 7. The method of approximation applies fairly well for the extreme case of 60° sweep and better correlation is obtained for wings with smaller angles of sweep. It is therefore suggested that the sidewash results for swept wings be approximated by reducing the unswept results by the ratio of the swept- and unswept-wing damping-in-roll derivatives.

Tail length.—For the normal range of tail positions investigated, the tail length was found to have a negligible effect on the sidewash angle. Results of calculations for tail lengths of 1 and 2 semispans are shown in figure 8. The tail length has a more important effect in determining the location of the sidewash-angle distribution with respect to the vertical tail, which is discussed subsequently.

Tail span.—In equation (11), the sidewash is seen to be a function of height above the trailing vortex sheet. In general, the sidewash decreases as the distance above the vortex sheet increases, as illustrated in figure 6. As the span of the vertical tail is increased, the sidewash on the tip sections becomes less and, if an average value of the sidewash over the tail were computed, the value would decrease somewhat with an increase in span for zero angle of attack.

FACTORS WHICH AFFECT THE DISPLACEMENT OF THE RESULTANT ANGULARITY DISTRIBUTION WITH RESPECT TO THE VERTICAL TAIL

The preceding section discussed factors which affect the magnitude of the sidewash angle with respect to the vortex sheet. This section discusses factors which affect the relative locations of the trailing vortex sheet at the tail and of the vertical-tail root with respect to the longitudinal axis and which thus affect the location of the resultant angularity distribution with respect to the vertical tail.

Angle of attack.—Three primary effects due to angle of attack are additional loading on the wing, displacement of the vertical tail, and displacement of the trailing vortex sheet. The symmetrical nature of the additional loading due to angle of attack results in no additional sidewash in the plane of symmetry from this effect, but the displacements of the tail and the trailing vortex sheet must be considered. The displacements of the vortex sheet and the vertical tail will be found relative to the longitudinal axis, which is the axis of roll.

The trailing vortex sheet moves in a downward direction with respect to the longitudinal axis, for a positive angle of attack. From equation (2), the displacement of the vortex sheet at the tail is

$$\frac{h_1}{b/2}=-\frac{l_t}{b/2}\tan\epsilon$$

The angle of downwash ϵ may be related to the angle of

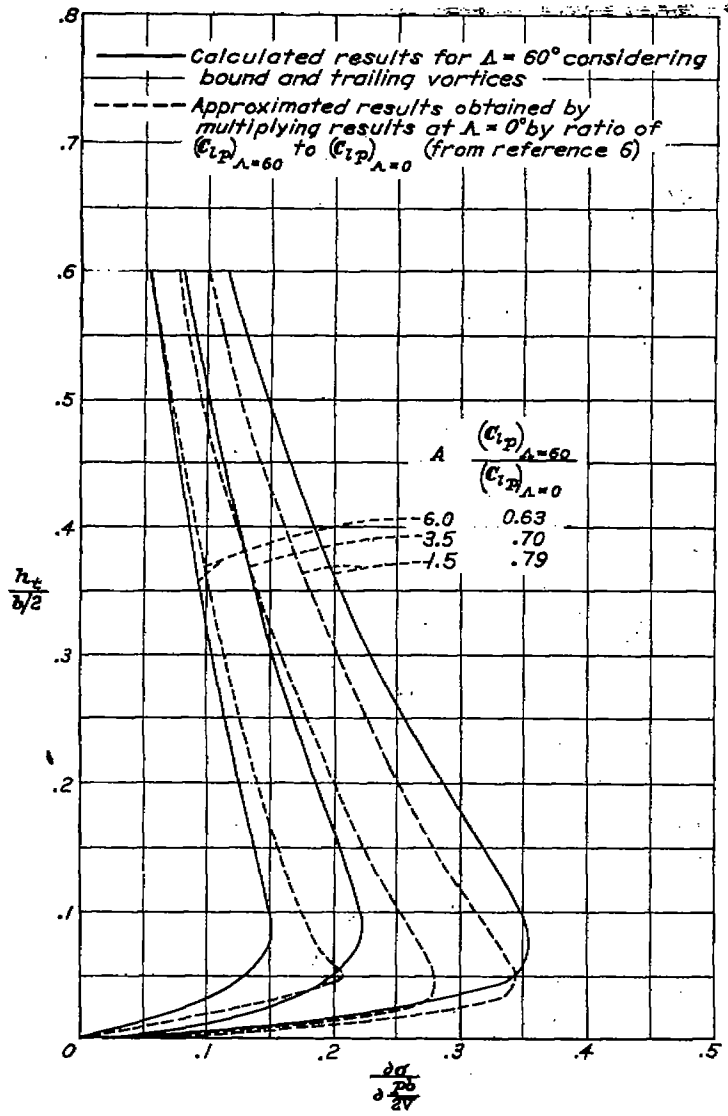

FIGURE 7.—Comparison of calculated sidewash results for Λ=60° considering bound and trailing vortices with approximated results. λ=0.5; $\frac{l_t}{b/2}$=1.0.

attack by the equation

$$\epsilon=\frac{d\epsilon}{d\alpha}\alpha \tag{14}$$

The displacement of the trailing vortex sheet at the tail expressed as a function of the angle of attack is

$$\frac{h_1}{b/2}=-\frac{l_t}{b/2}\tan\left(\frac{d\epsilon}{d\alpha}\alpha\right) \tag{15}$$

In discussing the displacement of the vertical tail, it is convenient to refer to a particular station on the tail, say the tail root. The displacement of the tail root is in a downward direction with respect to the longitudinal axis for positive angle of attack and is given by

$$-\frac{l_t}{b/2}\tan\alpha$$

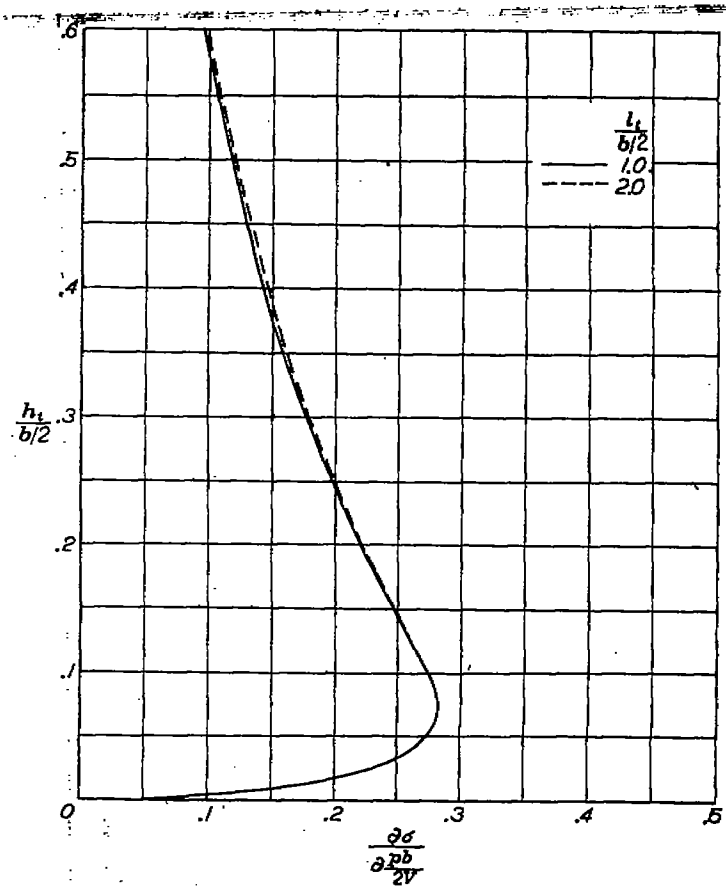

FIGURE 8.—The variation of sidewash-angle distribution with tail length. A=6.0; λ=1.0; Λ=0°; α=0°.

As mentioned previously, the resultant angularity distribution on the vertical tail can be found when both the resultant angularity distribution with respect to the longitudinal axis and the vertical-tail location with respect to the longitudinal axis are known.

The effect of changes in angle of attack on the sidewash at the vertical tail is shown in figure 9, in which the sidewash is presented as a function of height above the vertical-tail root. For this figure it was assumed that for zero angle of attack the vortex sheet and the tail root were in the same horizontal plane as the reference axis. The figure shows that the sidewash-angle distribution is shifted upward on the tail and thus that negative sidewash is induced on the lower portions of the vertical tail at positive angles of attack. It has been found that the decrease in sidewash angle with angle of attack is somewhat less than the increase in the geometric angle caused by the rolling tail, so that the resultant angularity at the vertical tail increases with angle of attack.

Geometrical construction.—Airplanes are so constructed that the vertical-tail root and the wing trailing edge do not usually lie in the same horizontal plane as the longitudinal axis at zero angle of attack. If the trailing-vortex-sheet location, which corresponds to the wing position, is above the longitudinal axis, with the tail root in the horizontal

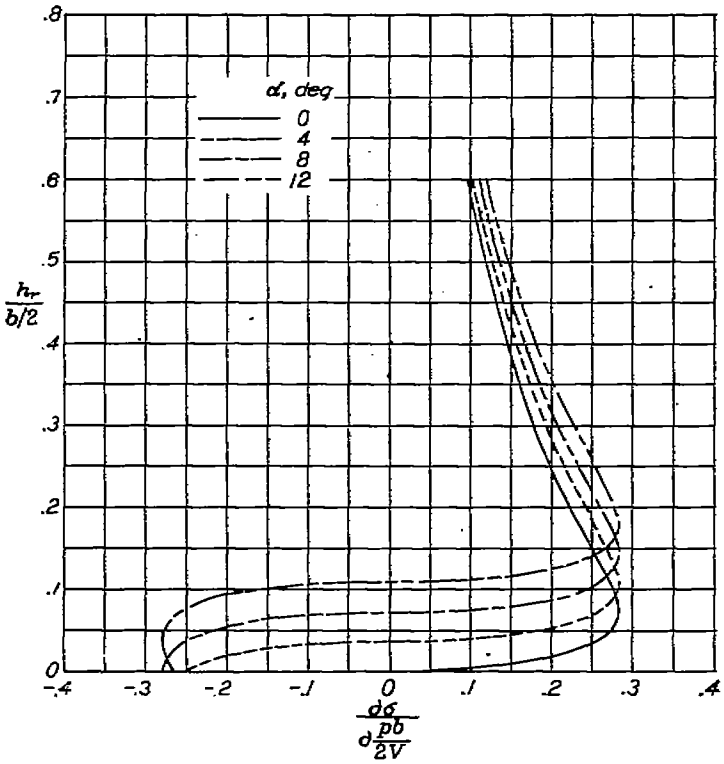

FIGURE 9.—Variation of sidewash-angle distribution at the vertical tail with angle of attack. $A=6.0$; $\lambda=1.0$; $\Lambda=0°$; $\frac{l_t}{b/2}=1.0$.

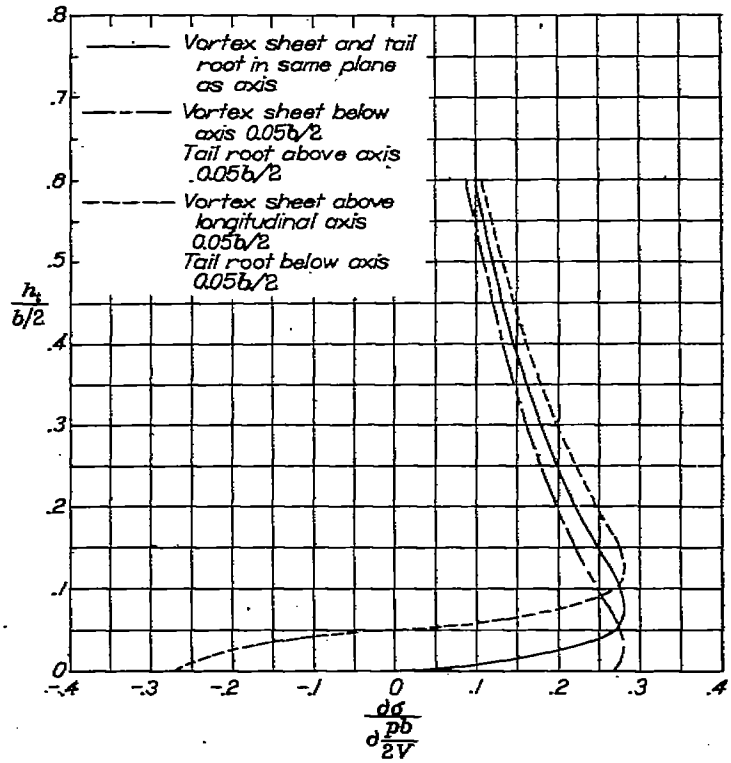

FIGURE 10.—The variation of sidewash-angle distribution on the vertical tail with position of the tail root and the trailing vortex sheet. $A=6.0$; $\Lambda=0°$; $\lambda=1.0$; $\alpha=0°$.

plane of the longitudinal axis, there will always be a reduction in the positive value of the effective sidewash angle on the tail. This reduction occurs because the sidewash is zero on the vortex sheet and becomes negative below the vortex sheet; thus, a negative increment is introduced when the vortex sheet is shifted upward on the tail. For vortex-sheet locations below the longitudinal axis, a slight decrease in the positive sidewash distribution occurs. These considerations are illustrated in figure 10.

When the tail root is above or below the longitudinal axis, with the vortex sheet in the plane of the axis, the effect on the angularity distribution at the tail is simply that of shifting the angularity distribution down or up by the amount of the displacement of the root. A displacement of the tail root above the reference axis has the same effect as a vortex-sheet displacement below the axis and vice versa.

Other factors.—For wings with flaps, the additional loading due to flap deflection is symmetrical and the contribution to the sidewash should be negligible according to the same argument as that for the additional angle-of-attack loading. However, the additional loading due to flap deflection increases the downwash behind the wing in the same manner as the angle-of-attack loading increases the downwash. This effect is difficult to estimate but should be accounted for when possible by using experimental values of the change in downwash angle with flap deflection.

It can be seen from expressions in the preceding sections that although changes in tail length had little effect on the sidewash calculations such changes are of importance in determining the resultant angularity distribution on the vertical tail.

APPLICATION

The vertical-tail contribution to the lateral-force-due-to-roll coefficient may be expressed in the form

$$(C_{Y_p})_t=\frac{\partial C_Y}{\partial \alpha_V}\frac{\partial \alpha_V}{\partial \frac{pb}{2V}}$$

and the corresponding expressions for yawing moment and rolling moment due to roll are obtained by multiplying the lateral-force expression by the proper moment arm. The general expressions for the application of the angularity results obtained herein to the calculation of the vertical-tail contributions to the rolling derivatives are

$$\left.\begin{aligned}(C_{Y_p})_t&=\frac{1}{S_W}\int_{Root}^{Tip}(c_{l_\alpha})_V\alpha_{V_p}c_V\,dh\\(C_{n_p})_t&=\frac{1}{S_W b}\int_{Root}^{Tip}(c_{l_\alpha})_V\alpha_{V_p}c_V(l_t'\cos\alpha+\bar{h}'\sin\alpha)\,dh\\(C_{l_p})_t&=\frac{1}{S_W b}\int_{Root}^{Tip}(c_{l_\alpha})_V\alpha_{V_p}c_V(\bar{h}'\cos\alpha-l_t'\sin\alpha)\,dh\end{aligned}\right\}\quad(16)$$

where

$$\alpha_{V_p}=-\frac{2}{b}(\bar{h}'\cos\alpha-l_t'\sin\alpha)+\frac{\partial\sigma}{\partial\frac{pb}{2V}}$$

and the distances l_t' and $\bar{h}'$ refer to the section centers of pressure. If the distribution of the vertical-tail section lift-curve slope for the particular flight attitude is known, the integrals in the preceding equations can be evaluated by graphical means by using a sufficient number of points over the vertical-tail span to give reasonably smooth curves. In the usual case, the section-lift-curve-slope distribution is not known and, also, the preceding method is somewhat lengthy. Past experience has shown that it is more convenient to replace the section lift-curve slope by a constant, the vertical-tail lift-curve slope, and to find an average tail angle of attack due to rolling that can be applied at the calculated center of pressure of the vertical tail. The average induced angle due to the rolling tail has been assumed in reference 1 to be simply that calculated at the center of pressure. There remains only to find an expression for $\left(\frac{\partial\sigma}{\partial\frac{pb}{2V}}\right)_{av}$ and then the tail contributions can be found from the following equations, which are similar to those of reference 2:

$$\left.\begin{aligned}
(C_{Y_p})_t&=(C_{L_\alpha})_V\frac{S_V}{S_W}\left[-\frac{2}{b}(\bar{h}\cos\alpha-l_t\sin\alpha)+\left(\frac{\partial\sigma}{\partial\frac{pb}{2V}}\right)_{av}\right]\\
(C_{n_p})_t&=-(C_{L_\alpha})_V\frac{S_V}{S_W}\left[\frac{1}{b}(\bar{h}\sin\alpha+l_t\cos\alpha)\right]\\
&\qquad\left[-\frac{2}{b}(\bar{h}\cos\alpha-l_t\sin\alpha)+\left(\frac{\partial\sigma}{\partial\frac{pb}{2V}}\right)_{av}\right]\\
(C_{l_p})_t&=(C_{L_\alpha})_V\frac{S_V}{S_W}\left[\frac{1}{b}(\bar{h}\cos\alpha-l_t\sin\alpha)\right]\\
&\qquad\left[-\frac{2}{b}(\bar{h}\cos\alpha-l_t\sin\alpha)+\left(\frac{\partial\sigma}{\partial\frac{pb}{2V}}\right)_{av}\right]
\end{aligned}\right\}\quad(17)$$

Values for $\left(\frac{\partial\sigma}{\partial\frac{pb}{2V}}\right)_{av}$ can be found by using the sidewash results presented in figure 6. Results of calculations for $\left(\frac{\partial\sigma}{\partial\frac{pb}{2V}}\right)_{av}$ (corresponding to wing aspect ratios of 3.5 and 6.0 and for taper ratios of from 0.5 to 1.0) for several tail spans are presented in figure 11. These calculations were made for the case where the vortex sheet and the vertical-tail root were in the same plane as the reference axis at zero angle of attack. Approximate corrections to $\left(\frac{\partial\sigma}{\partial\frac{pb}{2V}}\right)_{av}$ for vortex-

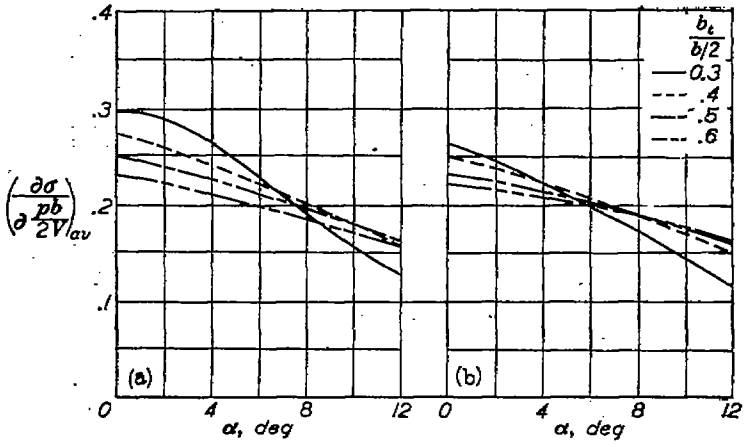

(a) $A=3.5$. (b) $A=6.0$.

FIGURE 11.—Charts for estimation of the average sidewash angle at the vertical tail. $\Lambda=0°$; $\lambda=0.5$ to 1.0; $\frac{l_t}{b/2}=1.0$.

sheet positions above the reference axis or for the tail root below the reference axis at zero angle of attack can be made by reducing the value of $\left(\frac{\partial\sigma}{\partial\frac{pb}{2V}}\right)_{av}$ obtained from figure 11 by the amount of the displacements, measured in semispans.

A comparison of calculated values of the vertical-tail contributions to the rolling derivatives with experimental data for the model of reference 2 is given in figure 12 (a). For the cases of the derivatives $(C_{Y_p})_t$ and $(C_{n_p})_t$, consideration of wing interference is of such importance as to change the sign of the calculated values so that fair agreement with the experimental data is obtained. The trend of the calculated results with angle of attack is in only fair agreement with the trend of the experimental data, probably because of additional sidewash due to the fuselage, which has not been accounted for in this analysis. The sidewash values used in the comparison are those obtained from figure 11 and are a function of the angle of attack. It is of interest to note that somewhat better agreement is obtained if the value of $\left(\frac{\partial\sigma}{\partial\frac{pb}{2V}}\right)_{av}$ calculated at zero angle of attack is used throughout the angle-of-attack range. Apparently the error in neglecting the variation of $\left(\frac{\partial\sigma}{\partial\frac{pb}{2V}}\right)_{av}$ with angle of attack partly offsets the error due to neglecting the fuselage; thus, the more simple application using a constant $\left(\frac{\partial\sigma}{\partial\frac{pb}{2V}}\right)_{av}$ gives the better results, for the particular model investigated.

The comparison of calculated and measured results for the swept-wing model shown in figure 12 (b) has the same general appearance as the comparison for the unswept wing.

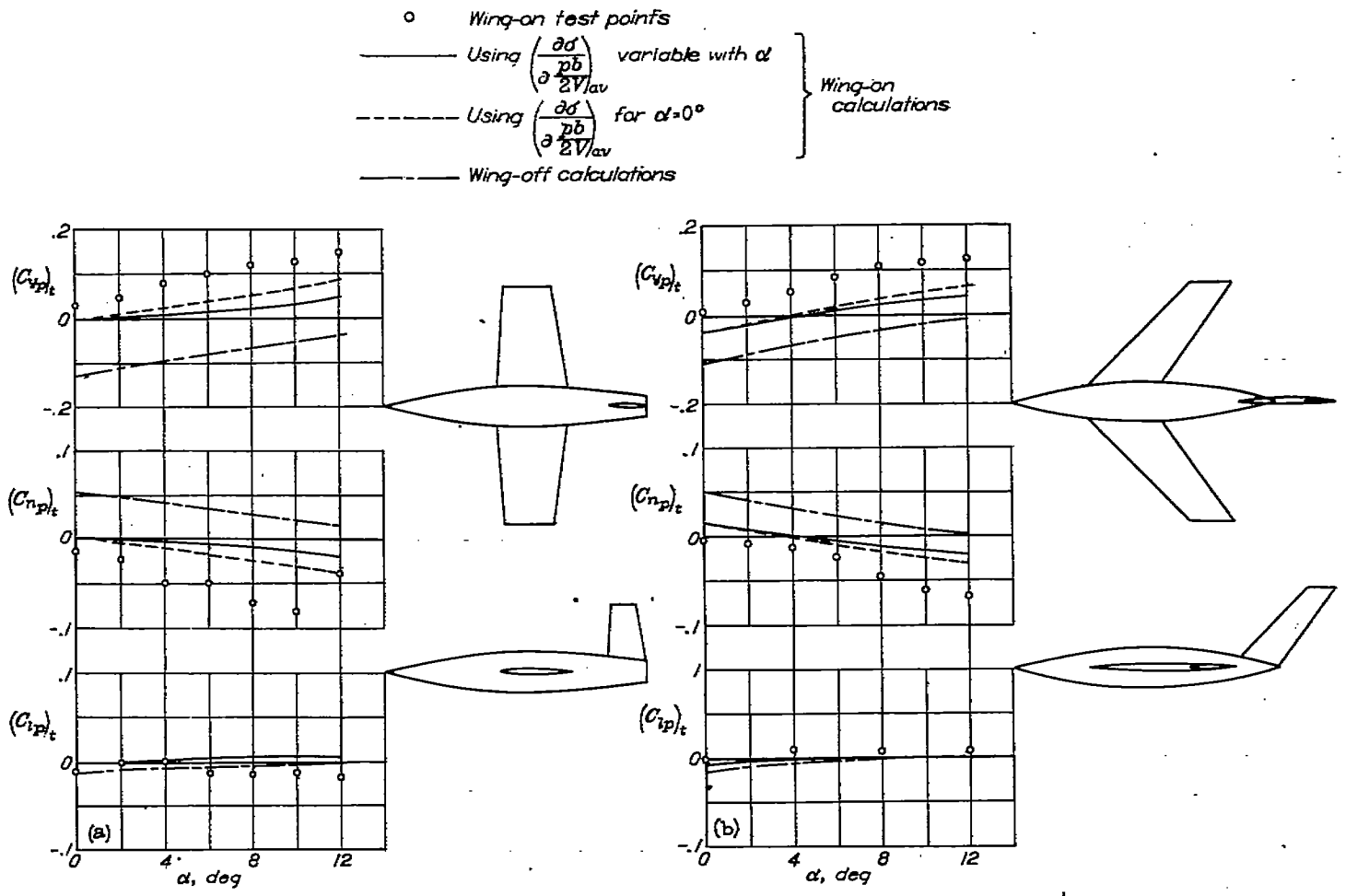

(a) Model of reference 2. $A=4.0$; $\Lambda=0°$; $\lambda=0.6$; $\frac{l_t}{b/2}=0.86$.

(b) Swept-wing model. $A=4.0$; $\Lambda=45°$; $\lambda=0.6$; $\frac{l_t}{b/2}=0.93$.

FIGURE 12.—Comparison of measured and calculated values of the tail contributions to the rolling derivatives. Horizontal tail off.

The calculated results presented in the figure were obtained from sidewash calculations considering the bound and trailing vortices of the swept wing, but approximated results obtained by means of the method suggested previously in the report gave essentially the same results as those presented in the figure.

Calculated values of $(C_{n_p})_t$ for a rectangular wing of aspect ratio 6.0 at zero angle of attack are presented in figure 13 as a function of the ratio of vertical-tail span to wing span. Measured values for $(C_{n_p})_t$ for a sting-mounted model with a small-diameter stick fuselage and two different vertical tails are also given in the figure. This comparison illustrates how the values of $(C_{n_p})_t$ may change sign with change in vertical-tail span and also gives an indication of how the calculated and measured results compare when the measured results are subject to very nearly the same conditions as those assumed in the calculations.

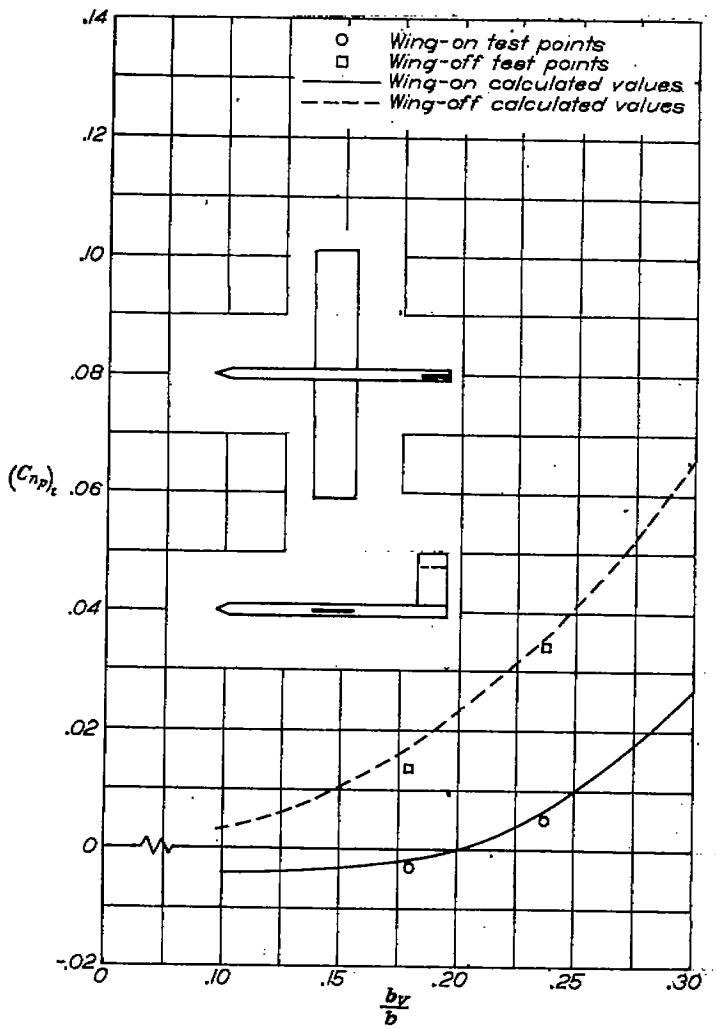

FIGURE 13.—Comparison of calculated with experimental values for a stick-fuselage model. $A=6.0$; $\lambda=1.0$; $\Lambda=0°$; $\frac{l_t}{b/2}=0.73$; $\alpha=0°$.

CONCLUDING REMARKS

The effect of wing interference on the tail contributions to the rolling derivatives of complete airplane configurations is determined by calculating the air-stream angularity at the vertical tail in rolling flight and finding the resultant forces and moments. The important factors in the determination of the angularity distribution on the vertical tail are wing plan form, vertical-tail span, and considerations associated with angle of attack and airplane geometry. A comparison of the calculated and experimental results indicates that a consideration of wing interference can be expected to be of such importance as to change the sign of the calculated values and that fair agreement with the available experimental data is obtained.

LANGLEY AERONAUTICAL LABORATORY,
NATIONAL ADVISORY COMMITTEE FOR AERONAUTICS,
LANGLEY FIELD, VA., *January 24, 1951.*

REFERENCES

1. Bamber, Millard J.: Effect of Some Present-Day Airplane Design Trends on Requirements for Lateral Stability. NACA TN 814, 1941.
2. Letko, William, and Riley, Donald R.: Effect of an Unswept Wing on the Contribution of Unswept-Tail Configurations to the Low-Speed Static- and Rolling-Stability Derivatives of a Midwing Airplane Model. NACA TN 2175, 1950.
3. Silverstein, Abe, Katzoff, S., and Bullivant, W. Kenneth: Downwash and Wake Behind Plain and Flapped Airfoils. NACA Rep. 651, 1939.
4. Spreiter, John R., and Sacks, Alvin H.: The Rolling Up of the Trailing Vortex Sheet and Its Effect on the Downwash Behind Wings. Jour. Aero. Sci., vol. 18, no. 1, Jan. 1951, pp. 21–32, 72.
5. Bird, John D.: Some Theoretical Low-Speed Span Loading Characteristics of Swept Wings in Roll and Sideslip. NACA Rep. 969, 1950. (Supersedes NACA TN 1839.)
6. Toll, Thomas A., and Queijo, M. J.: Approximate Relations and Charts for Low-Speed Stability Derivatives of Swept Wings. NACA TN 1581, 1948.